Nanoscale

Accepted Manuscript

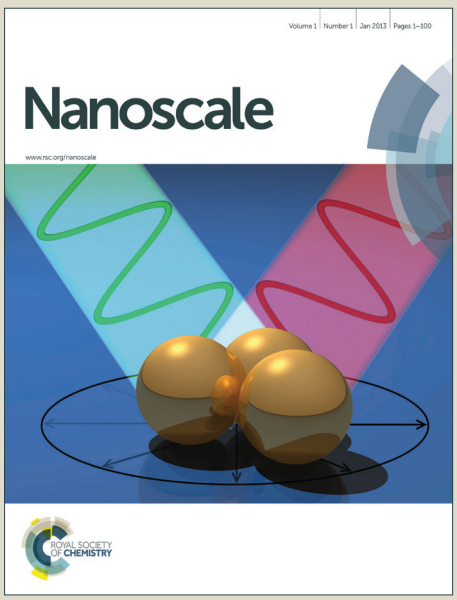

ROYAL SOCIETY OF CHEMISTRY

www.rsc.org/nanoscale

Journal Name

RSCPublishing

COMMUNICATION

Fabrication of Shape-Controlled Reduced Graphene Oxide Nanorings by Au@Pt Nanoring Lithography

Cite this: DOI: 10.1039/x0xx00000x

Received 00th January 2012,
Accepted 00th January 2012

DOI: 10.1039/x0xx00000x

www.rsc.org/

Ho Young Jang,[a] Hee-Jeong Jang, [b] Dae Keun Park[b] and Wan Soo Yun[b,1] and Sungho Park [a ,b, 1]

[1]Electronic mail: S. Park, spark72@skku.edu; W. Yun, ysyun87@skku.edu.

We fabricated a variety of reduced graphene oxide(RGO) nanoring arrays using Au@Pt nanoplates as a pattern mask. RGO nanoflakes are assembled into a 2-dimensional assembly at the water/oil interface, and then various shapes of Au@Pt nanoplates were utilized as a pattern mask in order to convert the RGO into circular, triangular, and hexagonal RGO nanorings.

Graphene, a honeycomb two-dimensional carbon structure, has attracted great attention for various applications such as transparent conducting electrodes (TCE),[1-3] supercapacitors,[4-6] and biosensors[7-9] because of its special properties. Since the first discovery of graphene in 2004, graphene has shown extraordinary properties such as high mobility, transparency, and flexibility. There are many methods for the synthesis of graphene, including chemical vapor deposition (CVD), chemical reduction of graphene oxide, and mechanical exfoliation from graphite flakes.

Furthermore, graphene has demonstrated potentially semiconducting properties at room temperature; however, this behavior is not appropriate for applications in electronic devices due to a lack of sufficient bandgap for the semiconducting behavior. The energy band gap of graphene, which is zero, has been widened by trimming the width of graphene,[10-14] and many researchers have studied means to widen the bandgap by modifying the structure of graphene to graphene nanoribbons (GNRs),[10, 13, 14] graphene nanomeshes (GNMs),[12] graphene nanorings (GRNRs)[11], and graphene quantum dots (GQDs).[15] These structures have shown semiconducting properties due to quantum confinement effects[13] and edge roughness.[16]

To fabricate graphene nanoribbons or nanomeshes with sub-15-nm width, E-beam lithography[17] and scanning tunneling microscopy (STM)[18] are often adopted. However, these methods are complicated and inquire sophisticated instruments. Most recently, Jiao et al. reported the fabrication of aligned graphene nanoribbons that were obtained when carbon nanotube side-walls were cut longitudinally by an argon (Ar) plasma etching process.[19] Also, Bai et al. attempted to fabricate graphene nanoribbons by using silicon nanowires (SiNW) as etching masks with oxygen plasma treatment.[20] Further, the properties of graphene nanoribbons were changed by tuning the width of the neck. As shown in these previously reported results, it is very important to fabricate graphene nanostructures with narrow widths to apply graphene to practical electronics applications. Recently, the graphene nanomeshes were obtained by nanosphere lithography masked with polymer beads such as poly(styrene-block-methyl methacrylate) (P(S-b-MMA))[12] and polystyrene.[21] Therefore, it is necessary to develop a facile method to pattern the graphene into specific shapes in order to facilitate further applications with graphene.

Herein, we report a shape-control fabrication method to produce reduced graphene oxide (RGO) nanorings that are approximately 10-nm wide from RGO flakes that are randomly dispersed in a solution using Au@Pt nanoplates as a pattern mask. Previously, we reported the shape-controlled synthesis of Au@Pt nanoplates.[22] We apply these unique nanostructures to the patterning process of RGO with narrow rim size. The utilized Au@Pt nanoplates have a thicker Pt rim coating on the Au core than on the center. During the O_2

plasmon etching, the central Au melts and Au@Pt nanoplates change their shape into Au/Pt nanorings, which is critical for the formation of RGO nanorings. The resulting RGO nanorings are characterized by scanning electron microscopy (SEM), atomic force microscopy (AFM), and Raman spectroscopy.

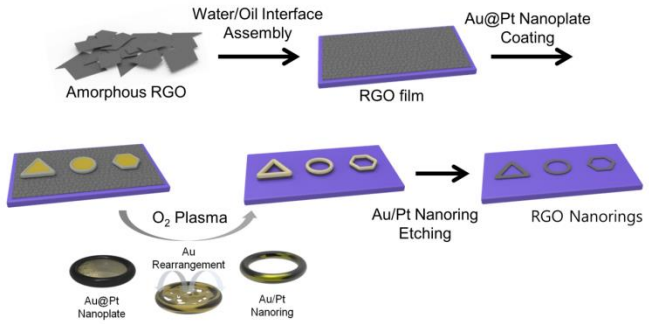

Figure 1 Schematic diagram of the fabrication of RGO nanoring arrays using Au@Pt nanoplates.

Figure 1 shows a schematic strategy for the fabrication process for shape-controlled RGO nanoring structures. First, RGO sheets were assembled into a well-ordered 2-dimensional assembly at the water/oil interface. The resulting films were horizontally lifted onto silicon substrates. RGO sheets were stabilized in water by negatively charged functional groups such as hydroxyl, carbonyl, and carboxyl moieties. In Figure 2A, the schematic diagrams show details related to production of uniform arrays of RGO sheets on substrates. First, hexane is poured on the top of the RGO solution to form a water/hexane interface, and ethanol was then added drop-wise to the water/hexane solution, resulting in RGO sheets assembled at the interface. This process is similar to the metal nanoparticle trapping at the water/oil interface.[23, 24] The dielectric constant of the RGO solution decreases when lower dielectric constant solvents such as ethanol are added. The surface energy of the RGO sheets decrease steadily when the amount of ethanol added is increased.

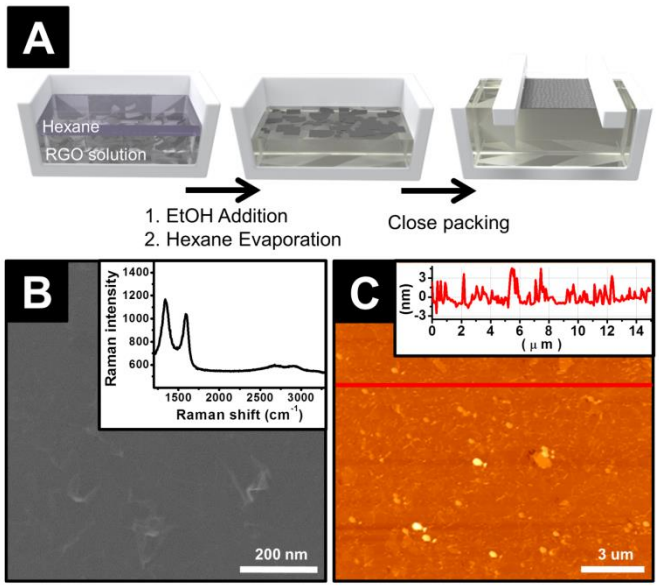

Figure 2 (A) Schematic representation of the RGO sheets film formation. (B) SEM image of RGO film. Inset graph shows Raman spectrum of RGO film. (C) AFM image of RGO film on SiO_2 substrates. Inset graph shows height profile along the red lines.

Also, the interfacial energy of the water/hexane interface decreases by the adsorption of RGO sheets at the interface. Lowering of the water/hexane interfacial energy is the driving force for entrapping RGO sheets. Then, the hexane is evaporated spontaneously leaving RGO sheets floating on the top of the water. The resulting RGO films are closely packed by two Teflon bars, as shown in panel A of Figure 2. The resulting film was transferred to a silicon substrate by horizontal lifting. Figure 2B shows an SEM image of RGO films on a SiO_2 wafer.

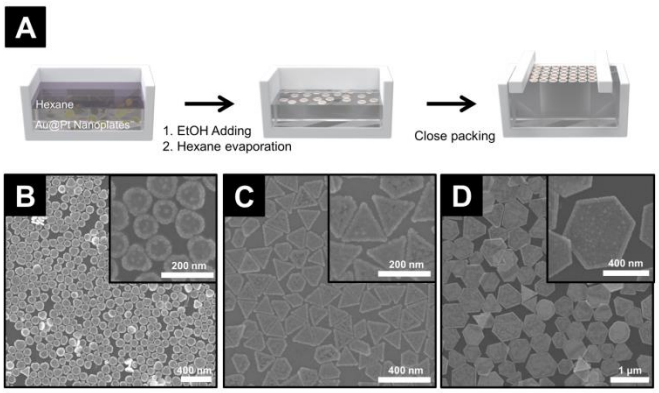

Figure 3 (A) Schematic representation of the Au@Pt nanoplates array film formation. SEM images of closed packed various Au@Pt nanoplates of (B) nanodisks, (C) nanoprisms, (D) nano hexagonal plates.

The inset in Figure 2B is the typical Raman spectral profile of an RGO film. RGO typically shows two sharpened peaks including a D peak (~1350 cm^{-1}) and a G peak (~1580 cm^{-1}), indicating lattice distortions and in-plane sp^2 carbon-carbon bond stretching motion, respectively. The intensity ratio of the two bands, I_D/I_G, is widely used to confirm the degree of disorder and crystallite size in graphitic materials. The typical intensity ratio (I_D/I_G) of RGO is known to be over 1 because of deoxygenation from graphene oxide. The splitting of the 2D peak (around 2700 cm^{-1}) indicates disordered stacking caused by single and few-layer graphene sheets. Figure 2C is an atomic force microscopy (AFM) image of the resulting RGO film. AFM images further prove the very smooth and uniform surface morphology of closed-packed RGO films. As shown in the line scans, the surface roughness is 2.5 nm, which is induced by the wrinkles at the edges of RGO sheets.

Then, Au@Pt nanoplates are placed on top of RGO films, as described in Figure 1. Various shapes of Au@Pt nanoplates are assembled into 2-dimensional arrays at the water/hexane interface by following a similar process as in the case of RGO films. The details of placing the Au@Pt nanoplates on top of the RGO film are described schematically in Figure 3A. First, hexane is poured on the top of the suspension of Au@Pt nanoplates in water, and then drop-wise addition of ethanol follows, leading to the assembly of Au@Pt nanoplates at the water/hexane interface. The density of Au@Pt nanoplates at the water/hexane interface could be controlled not only by the amount of ethanol added, but also by the control of concentration of 3-mercaptopropyltrimethoxysilane (MPTMS) in hexane. MPTMS plays a critical role for forming monolayer and uniform arrangement of Au@Pt nanodisks. In our previous paper,

coating nanoparticle surfaces with organic molecules at a water/oil interface is important for forming highly ordered close-packed nanoparticle arrays.[25] When the concentration of MPTMS is 1×10^{-7} M in the hexane layer, the packing density of Au@Pt nanoplates is low because of the repulsive force between Au@Pt nanoplates. On the other hand, when an adequate concentration (1×10^{-6} M) of MPTMS is added in the hexane layer, the surface charge of Au@Pt nanoplates decreases enough to allow for the existence of Au@Pt nanoplates next to each other due to the decrease in their electrostatic repulsive force. Thus, Au@Pt nanoplates are assembled uniformly at the water/hexane interface.

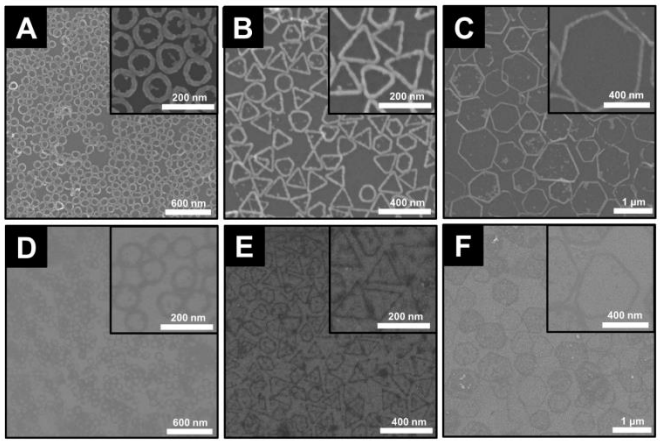

Figure 4 SEM images of various Au/Pt alloy nanostructure array films of (A) nanoring, (B) triangular nanoring, and (C) hexagonal nanoring shapes, and the corresponding SEM images of (D) RGO nanoring, (E) RGO triangular and (F) RGO hexagonal nanoring array films.

Various shapes of Au@Pt nanoplates assembled in well-ordered 2-dimensional arrays are shown in Figure 3B-D. However, excess MPTMS coating on Au@Pt nanoplates leads to the formation of multilayer of Au@Pt nanoplates because it converts an electrostatic repulsive force into a van der Waals attraction by forming organic coating layers around the Au@Pt nanoplates. Typically, when an excessive amount of MPTMS (1×10^{-5} M) is added in hexane, the surfaces of Au@Pt nanoplates are fully covered with MPTMS. In this case, the Au@Pt nanoplates form multilayers (Supporting Information Figure S1 A-C). It is noteworthy that the formation of a monolayer arrangement of Au@Pt nanoplates is critical later in making RGO nanorings.

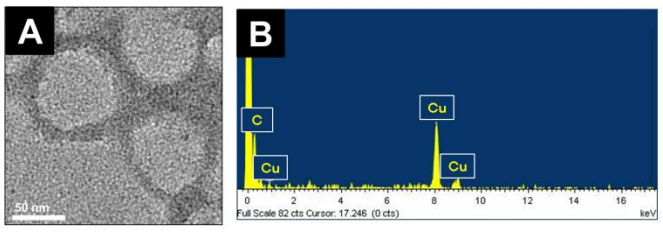

Figure 5 (A) TEM image of RGO nanorings and (B) corresponding EDS spectrum. Cu element originates from TEM grid.

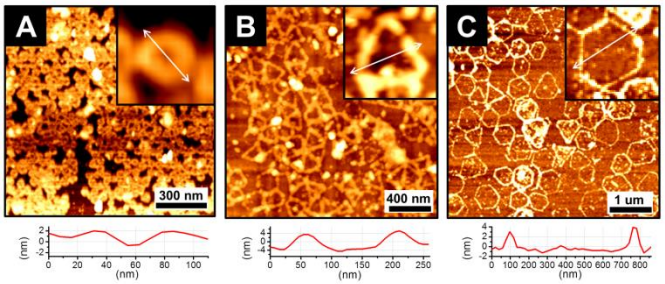

Figure 6 AFM images of RGO (A) nanoring, (B) triangular nanoring and (C) hexagonal nanoring structures on SiO_2 substrates. Graphs indicate the line mapping of the one RGO nanoring structures corresponding inset AFM image.

By controlling the concentration of MPTMS in the hexane layer and the amount of ethanol added to the Teflon cell, a 2-dimensional monolayer array of Au@Pt nanoplates could be formed and transferred to the top of RGO films by horizontal lifting.

As a next step, the RGO film covered by the 2-dimensional monolayer array of Au@Pt nanoplates was placed under O_2 plasma treatment, where the exposed RGO undergoes decomposition and the Au@Pt nanoplates transform their shape into nanorings (Figure 1). When the Au@Pt nanoplate was transformed to Au/Pt nanoring structure, uncovered RGO portions were also etched out by O_2 plasma. During O_2 plasma treatment, the center part of Au at the Au@Pt nanoplates melted away and rearranged with Pt, generating Au/Pt nanorings. The Pt rim survives due to its higher melting temperature than that of Au.[26] The shape transformation from nanoplates to nanorings is the critical step for the formation of RGO nanorings.

The RGO films covered by the 2-dimensional monolayer array of various shapes of Au/Pt nanorings are shown in Figure 4A-C. The rim thickness of each Au/Pt nanoring is 21±2 nm for circular nanorings, 22±2 nm for triangular nanorings, and 29±4 nm for hexagonal nanorings. As compared to Figure 3B-D, all Au@Pt nanoplates are converted to Au/Pt nanorings, showing the void at the center of the nanorings. The thickness of the Pt part in Au@Pt nanoplates is uniform over the entire sample, which is shown in Figure 4 A-C with a narrow size distribution (thickness of rim ~ 21±2, 22±2, and 29±4 nm for Au/Pt nanorings shown in panel A, B, and C, respectively). Then, Au/Pt nanorings were etched out using an aqua regia solution for 3 h, finally resulting in RGO nanoring arrays on wafers (figure 4D-F). SEM images of various RGO nanoring structures indicate the average widths of the rim are 15±3 for circular RGO nanorings, and 12±2 nm for triangrular RGO nanorings, and 20±4 nm for RGO hexagonal nanorings, which is smaller than the rim thickness of Au@Pt nanorings. A typical TEM image shows the detailed morphology of RGO nanorings and their corresponding EDS spectrum representing that Pt and Au elements are completely removed after chemical etching of Pt and Au. (Figure 5)

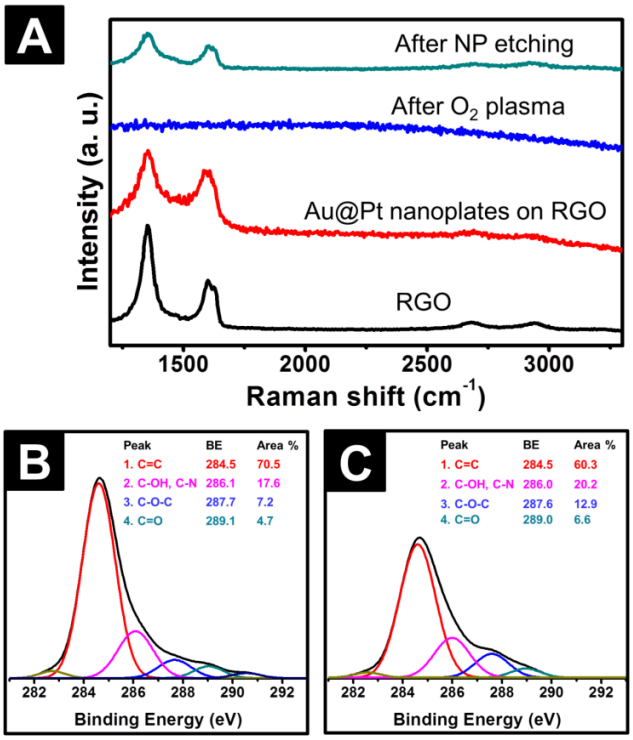

Figure 7 (A) Raman spectra of each steps in RGO nanoring fabrication. High resolution XPS spectra of the C 1s region of reduced graphene oxide (B) and RGO nanoring (C) samples on SiO_2 substrate.

A detailed analysis of RGO nanorings was carried out by non-contact mode atomic force microscopy (AFM) (Figure 6). The images taken by AFM show RGO nanoring, triangular and hexagonal nanoring films. As shown in the line scan of RGO nanorings, the thickness of the RGO nanoring is 2.3 (±1.1) nm, which indicates a few layers of RGO film. Thicknesses of RGO triangular and hexagonal nanoring films were 6.7 (±1.4) nm and 3.8 (±1.5) nm respectively. As previously emphasized, the Pt rims of Au@Pt nanoplates play a critical role as a pattern mask in the process of RGO nanoring fabrication. When a small amount of Pt is deposited at the edge of the Au disks, the disks aggregate with other Au@Pt nanodisks during O_2 plasma treatment (Figure S2 A-C). Consequently, there is no RGO nanoring formation, and instead the RGO flakes are formed by following the shape of Au@Pt nanoplates. In contrast, when the thickness of the Pt wall is too high, the Au cores do not disappear during the O_2 plasma treatment, leading to the formation of RGO nanodot structures (Figure S2 D-F). We further characterized as-prepared RGO nanorings corresponding to each process by Raman spectroscopy (Figure 7).

First, the intrinsic RGO film shows typical Raman features showing a sharpened D peak and a G peak. When the Au@Pt nanodisks are coated on the RGO film, Raman signals are slightly dampened since Au@Pt nanodisks block the RGO. After O_2 plasma treatment, we can see Raman features that have disappeared (blue line), which indicates RGO is etched where Au@Pt nanodisks do not cover. The only area covered by Au@Pt nanodisks remains as RGO nanorings underneath Au/Pt alloy nanorings. Finally, we retain RGO nanoring features (green line) with a Raman spectrum profile similar to pristine RGO films. Figures 7B and 7C show XPS spectra of RGO and RGO nanoring films, respectively. RGO films show four components centered at 284.6 eV, 286.1 eV, 287.7 eV, and 289.1 eV. These are attributed to C-C bonds, which are the most dominant peaks in non-oxidized carbon species, C in epoxy, alkoxy, and the carbonyl functional group, respectively. The low intensity of C-O and C=O peaks for the RGO film indicates considerable de-oxygenation during the reduction process and a large portion of C=C bonds in the total carbon bonds. A higher portion of C=C bonding indicates that this sample is successfully reduced from graphene oxide. As RGO nanorings are fabricated, the intensity of C=C bonds decreases significantly, while oxygen functional groups such as epoxy and carbonyl increase, in comparison with intrinsic RGO. This is because RGO nanorings have more edge boundaries than intrinsic RGO with more oxygen functional groups.

Conclusions

In conclusion, we fabricated RGO nanoring arrays with sub-10-nanometer width on SiO_2 substrates by O_2 plasma lithography using Au@Pt nanoplates as a pattern mask. AFM analysis demonstrates that the RGO nanorings are composed of few-layer graphene stacks, and XPS analysis supports the existence of RGO nanorings. The pattering process was monitored by Raman spectroscopy. This method, graphene trimming using a nanoplate, is very simple and has strong potential to contribute to future graphene electronic and optic studies for the development of carbon-based nanotransistors and nanophotonics

Acknowledgments

This work was supported by the National Research Foundation of Korea (National Leading Research Lab:2012R1A2A1A03670370)

Notes and references

[a] Department of Energy Science, Sungkyunkwan University, Suwon, 440-746, South Korea.
[b] Department of Chemistry, Sungkyunkwan University, Suwon, 440-746, South Korea.

Electronic Supplementary Information (ESI) available: [detailed experimental sections, additional SEM images]. See DOI: 10.1039/c000000x/

REFERENCES

1. X. S. Li, Y. W. Zhu, W. W. Cai, M. Borysiak, B. Y. Han, D. Chen, R. D. Piner, L. Colombo and R. S. Ruoff, *Nano Lett*, 2009, 9, 4359-4363.
2. K. S. Kim, Y. Zhao, H. Jang, S. Y. Lee, J. M. Kim, K. S. Kim, J. H. Ahn, P. Kim, J. Y. Choi and B. H. Hong, *Nature*, 2009, 457, 706-710.
3. G. Eda, G. Fanchini and M. Chhowalla, *Nat Nanotechnol*, 2008, 3, 270-274.
4. J. J. Yoo, K. Balakrishnan, J. S. Huang, V. Meunier, B. G. Sumpter, A. Srivastava, M. Conway, A. L. M. Reddy, J. Yu, R. Vajtai and P. M. Ajayan, *Nano Lett*, 2011, 11, 1423-1427.

5. C. G. Liu, Z. N. Yu, D. Neff, A. Zhamu and B. Z. Jang, *Nano Lett*, 2010, 10, 4863-4868.
6. Y. Wang, Z. Q. Shi, Y. Huang, Y. F. Ma, C. Y. Wang, M. M. Chen and Y. S. Chen, *J Phys Chem C*, 2009, 113, 13103-13107.
7. L. Wu, H. S. Chu, W. S. Koh and E. P. Li, *Opt Express*, 2010, 18, 14395-14400.
8. Y. X. Huang, X. C. Dong, Y. M. Shi, C. M. Li, L. J. Li and P. Chen, *Nanoscale*, 2010, 2, 1485-1488.
9. Y. Liu, D. S. Yu, C. Zeng, Z. C. Miao and L. M. Dai, *Langmuir*, 2010, 26, 6158-6160.
10. X. L. Li, X. R. Wang, L. Zhang, S. W. Lee and H. J. Dai, *Science*, 2008, 319, 1229-1232.
11. Y. Pak, H. Jeong, K. H. Lee, H. Song, T. Kwon, J. Park, W. Park, M. S. Jeong, T. Lee, S. Seo and G. Y. Jung, *Adv Mater*, 2013, 25, 199-204.
12. J. W. Bai, X. Zhong, S. Jiang, Y. Huang and X. F. Duan, *Nat Nanotechnol*, 2010, 5, 190-194.
13. M. Y. Han, B. Ozyilmaz, Y. B. Zhang and P. Kim, *Phys Rev Lett*, 2007, 98, 206805.
14. Y. W. Son, M. L. Cohen and S. G. Louie, *Nature*, 2006, 444, 347-349.
15. L. A. Ponomarenko, F. Schedin, M. I. Katsnelson, R. Yang, E. W. Hill, K. S. Novoselov and A. K. Geim, *Science*, 2008, 320, 356-358.
16. D. A. Areshkin, D. Gunlycke and C. T. White, *Nano Lett*, 2007, 7, 204-210.
17. B. Ozyilmaz, P. Jarillo-Herrero, D. Efetov and P. Kim, *Appl Phys Lett*, 2007, 91, 192107.
18. L. Tapaszto, G. Dobrik, P. Lambin and L. P. Biro, *Nat Nanotechnol*, 2008, 3, 397-401.
19. L. Y. Jiao, L. Zhang, X. R. Wang, G. Diankov and H. J. Dai, *Nature*, 2009, 458, 877-880.
20. J. W. Bai, X. F. Duan and Y. Huang, *Nano Lett*, 2009, 9, 2083-2087.
21. L. Liu, Y. L. Zhang, W. L. Wang, C. Z. Gu, X. D. Bai and E. G. Wang, *Adv Mater*, 2011, 23, 1246-1251.
22. H.-J. Jang, S. Hong, S. Ham, K. L. Shuford and S. Park, *Nanoscale*, 2014, 6, 7339-7345.
23. Y. K. Park, S. H. Yoo and S. Park, *Langmuir*, 2007, 23, 10505-10510.
24. Y. K. Park and S. Park, *Chem Mater*, 2008, 20, 2388-2393.
25. Y. Jung, Y. K. Park, S. Park and S. K. Kim, *Anal Chim Acta*, 2007, 602, 236-243.
26. C. S. Ah, S. J. Kim and D. J. Jang, *J Phys Chem B*, 2006, 110, 5486-5489.